Proceedings of the ASME 2021 International Design Engineering Technical Conferences & Computers and Information in Engineering Conference
IDETC/CIE 2021
August 17-20, 2021, Virtual

IDETC2021-70551

INSECT WING BUCKLING INFLUENCES STRESS AND STABILITY DURING COLLISIONS

Mark Jankauski
Assistant Professor, Montana State University
mark.jankauski@montana.edu

Ryan Schwab
Graduate Researcher, Montana State University
rschwab03@gmail.com

Cailin Casey
Graduate Researcher, Montana State University
cailin.casey@student.montana.edu

Andrew Mountcastle
Assistant Professor, Bates College
amountca@bates.edu

ABSTRACT

Flapping insect wings frequently collide with vegetation and other obstacles during flight. Repeated collisions may irreversibly damage the insect wing, thereby compromising the insect's ability to fly. Further, reaction torques caused by the collision may destabilize the insect and hinder its ability to maneuver. To mitigate the adverse effects of impact, some insect wings are equipped with a flexible joint called a "costal break." The costal break buckles once it exceeds a critical angle, which is believed to improve flight stability and prevent irreversible wing damage. However, to our knowledge, there are no models to predict the dynamics of the costal break. Through this research, we develop a simple model of an insect wing with a costal break. The wing was modeled as two beams interconnected by a torsional spring, where the stiffness of the torsional spring instantaneously decreases once it has exceeded a critical angle. We conducted a series of static tests to approximate model parameters. Then, we used numerical simulation to estimate the peak stresses and reaction moments experienced by the wing during a collision. We found that costal break increased the wing's natural frequency by about 50% compared to a homogeneous wing and thus reduced the stress associated with normal flapping. Buckling did not significantly affect peak stresses during collision. Joint buckling reduced the peak reaction moment by about 32%, suggesting that the costal break enhances flight stability.

INTRODUCTION

Insect wings are complex structures that serve multiple functions. Most notably, flapping wings produce the aerodynamic forces required for flight, such as lift and thrust which are predominantly generated by the wing's rigid body rotation [1]. Smaller wing deformation superimposed on larger rigid body motion is believed to augment aerodynamic force generation [2] and power economy [3]. At the same time, wings may play a role in sensing. Hawkmoth *Manduca sexta* wings are imbued with mechanoreceptors called campaniform sensilla, and the feedback encoded by these mechanoreceptors is believed to facilitate postural control [4]. Wings are therefore essential to flight, which enables insects to forage, locate food sources, escape predators, and in some cases, predate.

Because of the wing's importance to flight, irreversible wing damage may drastically reduce an insect's likelihood of survival. Wing damage has been shown to increase mortality rates in both honeybees [5] and bumblebees [6]. The increase in mortality rate may stem from the compromised aerodynamics. Wing area loss has been correlated to a decline in vertical accelerations in dragonflies [7] and is believed to inhibit maneuverability in bumblebees [8]. Loss of peak accelerations and maneuverability could affect an insect's ability to evade predators, navigate complex environments or cope with aerodynamic disturbances, such as turbulence or wind. In addition to aerodynamic repercussions, wing

damage may incur increased energetic costs. Lyu et al. estimated that unilateral wing damage in phorid flies increased the power required to flap the damaged wing up to 40% relative to the intact wing [9]. This increase in power consumption results from an increase in flapping amplitude of the damaged wing, where the increased flapping amplitude is necessary to generate aerodynamic forces comparable to the intact wing.

Wing damage may arise for a variety of reasons, though a predominant cause appears to be collisions with vegetation during foraging behavior. Foster and Cartar filmed bumblebees foraging in their natural habitat, and found wings that collided with vegetation frequently suffered more area loss relative to wings with less frequent collisions [10]. Mountcastle and Combes investigated wing loss in a more controlled setting, and used a motor to automate wing collisions at a regular interval [11]. They found that after the wing experienced nearly 780,000 collisions, the estimated number of collisions a wing may experience over the lifetime of the bumblebee, the wingtip lost approximately 20% of its area. In addition to area loss, wings may experience other types of damage, such as cracking and surface wear [12].

Interestingly, some insects employ strategies to reduce the damage their wings experience during collision. The wings of many hymeonopterans (bees and wasps) are equipped with a flexible joint located along the leading edge vein [13] (Fig. 1). This joint is called the costal break and exists in healthy, undamaged wings. Relatively little is known about the geometry or material characteristics of the costal break and surrounding regions, but research indicates that it behaves as a flexible joint that buckles once it experiences a critical angle [14], and this buckling appears to reduce the damage the wing experiences during collision. Mountcastle and Combes tested normal yellowjacket wings and yellowjacket wings with splinted costal breaks in a controlled collision apparatus and found that the normal wings experienced less area loss relative to the splinted wings [11]. Given its benefits in insects, the costal break damage mitigation feature has begun to be emulated in engineering design [15].

In addition to reducing wing damage, the costal break may also improve insect flight stability. The external forces generated when a wing strikes an object may produce a large reaction torque on the insect body. Depending on where the wing is in its stroke phase, this reaction torque may destabilize the insect by imparting an angular velocity to its body. The costal break may lessen the amount of force transmitted from the point of impact to the insect body, thereby reducing the body's post-collision angular velocity. While there is no conclusive evidence that the costal break improves stability in live insects, a buckling feature on an insect-scale flapping wing micro air vehicle has been shown to lessen the aircraft body's post-collision yaw rate substantially [14].

However, to the best of our knowledge, there are no mathematical models that estimate the damage-minimizing or stability benefits conferred by the costal break. The purpose of the present work is therefore to develop a simple model of an insect wing embedded with a costal break to predict its dynamics during a collision. We are specifically interested in estimating the peak stresses and reaction moments experienced by the wing. We acknowledge that this preliminary model is greatly simplified and does not fully capture the complexity of the insect wing, however we believe it is a reasonable starting place to understand the fundamental dynamic behavior of the costal break. Some of the most significant model assumptions include:

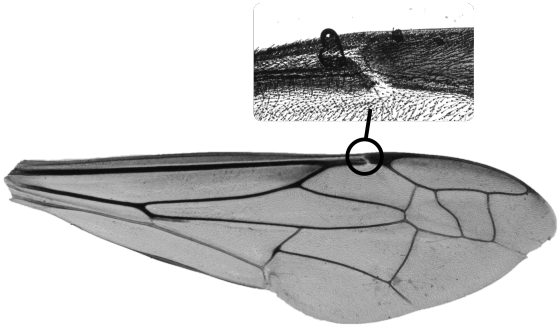

FIGURE 1. IMAGE OF YELLOWJACKET WING COSTAL BREAK. THE COSTAL BREAK TYPICALLY BUCKLES SUCH THAT THE WING BENDS OUT-OF-PLANE. NOTE THAT THIS IS NOT THE EXACT WING TESTED IN THIS WORK.

1. The wing is reduced to a system comprised of two beams interconnected by a torsional spring representative of the costal break. The material and geometric properties of the two beams, which represent the portion of the wing proximal and distal of the costal break, are assumed homogeneous.
2. The static testing used to tune model parameters considers dried wings. Desiccation is known to influence the wing's absolute material properties.
3. The costal break model is quasi-static and does not account for rate-dependent effects.
4. We consider only out-of-plane bending of the wing and therefore restrict the costal break to rotate only in one direction.

The remainder of the paper is organized as follows. First, we derive the model of the insect wing with costal break. We then detail a series of static force-displacement tests conducted to tune model parameters. Next, we conduct numerical studies to better understand how the wing's dynamics are influenced by the costal break. We conclude by discussing implications and future directions of the present work.

THEORY

Here, we derive a mathematical model to predict the deformation of a structure representative of an insect wing with a costal break.

The wing is comprised of two flexible beams interconnected by a torsional spring. Similar models have been used to model the dynamics of cracked beams [16–18], and thus the following provides only a brief summary of the model derivation. For a more detailed derivation, the reader is encouraged to refer to the above references.

The wing model is shown in Fig. 2. We denote the left beam and right beam as beam 1 and 2, respectively. Beam 1 represents the portion of wing proximal to the insect body, and beam 2 represents the distal portion of the wing. The beams are of lengths L_1 and L_2, and the position along each beam is described by x_1 and x_2. W_1 and W_2 denote the beam's infinitesimal transverse displacement. The beams are connected by a torsional spring of stiffness k_T. Assuming each beam has homogeneous material properties and cross sectional area, and that shear deformations are negligible, the partial differential equation governing the beam's transverse displacement [19] is

$$E_i I_i \frac{\partial^4 W(x_i,t)}{\partial x_i^4} + \rho_i A_i \frac{\partial^2 W(x_i,t)}{\partial t^2} = F_i(x_i,t) \tag{1}$$

where $i = 1,2$ and represents the left or right beam respectively, E is the Young's modulus, I is the area moment of inertia, A is the cross-sectional area, ρ is the mass density, F is a transverse force per unit length dependent on space and time, and t is time. The no displacement, no rotation boundary conditions at the fixed edge of the beam 1 are

$$W_1(0) = 0 \tag{2}$$
$$W_1'(0) = 0 \tag{3}$$

where $'$ denotes a first-order spatial derivative, $''$ denotes a second-order spatial derivative and so on. The no moment, no shear boundary conditions at the free edge of beam 2 are

$$W_2''(L_2) = 0 \tag{4}$$
$$W_2'''(L_2) = 0 \tag{5}$$

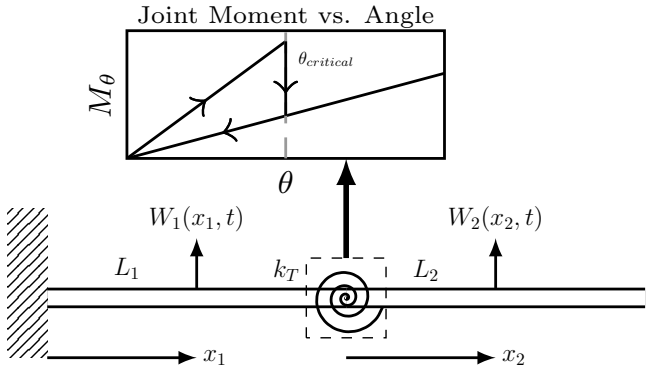

FIGURE 2. SIMPLE SCHEMATIC OF INSECT VEIN WITH COSTAL REPRESENTED BY TWO FLEXIBLE BEAMS CONNECTED BY A TORSIONAL SPRING.

At the torsional spring, the beam's transverse displacements, moments and shear are continuous, which gives

$$W_1(L_1) = W_2(0) \tag{6}$$
$$W_1''(L_1) = W_2''(0) \tag{7}$$
$$W_1'''(L_1) = W_2'''(0) \tag{8}$$

Lastly, compatibility at the torsional spring implies that

$$K_T \underbrace{[W_1'(L_1) - W_2'(0)]}_{\theta} + E_1 I_1 W_1''(L_1) = 0 \tag{9}$$

where θ is the angle of the torsional spring. This boundary condition permits that the slope be discontinuous at the torsional spring. The bending moment M and compressive/tensile stress σ internal to the deformed beams are

$$M_i(x_i) = E_i I_i \frac{d^2 W_i(x_i)}{dx_i^2} \tag{10}$$
$$\sigma_i(x_i) = \frac{z M_i(x_i)}{I_i} \tag{11}$$

where z is the distance from the beam's neutral axis to a point of interest. We use maximum stress as a proxy to identify how severely the wing may be damaged during collision. Lastly, we assume that the torsional spring has a linear stiffness defined by k_T. Once the joint angle has exceeded a critical angle $\theta_{critical}$, the "costal break" torsional spring buckles and its stiffness instantaneously switches to αk_T (Fig. 2), where α is a non-dimensional post-buckling stiffness scaling factor to be determined. We assume that the torsional spring stiffness remains αk_T until the joint angle returns to zero, and that the stiffness of the torsional spring is αk_T if $\theta > \theta_{critical}$. This is consistent with what we found in the static tests detailed in the following section.

For practical implementation, we discretize the continuous model in Eq. 1 to form a multiple-degree-of-freedom system comprised of interconnected finite beam elements [20] as

$$\mathbf{M}\ddot{\mathbf{q}} + \mathbf{C}\dot{\mathbf{q}} + \mathbf{K}\mathbf{q} = \mathbf{F}(t) \tag{12}$$

where $\mathbf{M}$, $\mathbf{C}$ and $\mathbf{K}$ are the system's mass, damping, and stiffness matrices respectively and $\mathbf{F}$ is an external force vector. Note that

the damping matrix is not explicit to the continuous formulation and is instead added to stabilize the dynamic solutions later in this manuscript. We assume the damping matrix is proportionally damped such that $\mathbf{C} = \alpha\mathbf{K} + \beta\mathbf{M}$, where α, β are constants tuned such that beam systems first two vibration modes of the beam system have modal damping ratios of 5%. Lastly, state vector $\mathbf{q}$ is $\mathbf{q} = [w_1,\ \theta_1,\ w_2,\ \theta_2, \ldots w_n,\ \theta_n]^T$, where w and θ are the beam elements transverse displacement and rotation, respectively. We use 100 beam elements to represent the system, which is sufficient to show convergence of the assembly's first four natural frequencies (Fig. 3). The costal break is represented as a sprung nodal hinge connecting two beam elements.

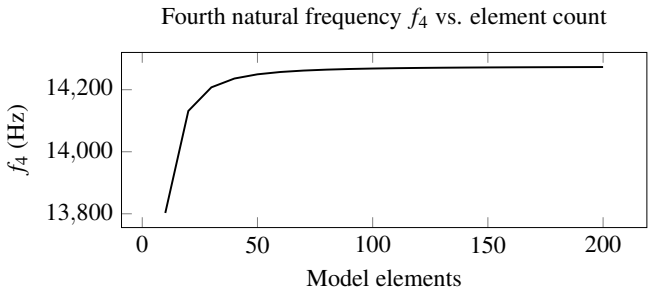

FIGURE 3. FOURTH NATURAL FREQUENCY VS. ELEMENT COUNT SHOWS CONVERGENCE. NOTE THAT THE LOWER NATURAL FREQUENCIES CONVERGE MORE QUICKLY.

STATIC EXPERIMENTS

We conducted a series of static experiments to estimate the wing's effective cross sectional area A, area moment of inertia I, Young's modulus E as well as the costal break's effective pre and post-buckling stiffness K_T and αK_T. These experiments were conducted on desiccated wings, where desiccation has been shown to increase wing stiffness in other contexts [21]. The benefit of working with dried wings is that their material properties are stable and do not change with time, which reduces the time sensitivity of the experiments. However, we stress that the flexible rigidity determined through this approach is likely several times higher than the flexural stiffness in fresh insect wings.

We first estimate the wing's effective cross sectional area and area moment of inertia through microscopy. We captured yellowjacket wasps *Vespula pensylvanica* using traps baited with Heptyl Butyrate and water. Captured wasps were euthanized with ethyl acetate and frozen. Wasps were removed from the freezer and let to dry prior to experimentation and their wings were removed using dissection scissors. In order to estimate the cross sectional area A and area moment of inertia I, we made slides from the wing pressed between two glass slips. Images for analysis were taken using the Nikon Eclipse E800 microscope and the infinity 2 color microscope camera. We hypothesize that the leading edge vein is the wing's predominant load bearing

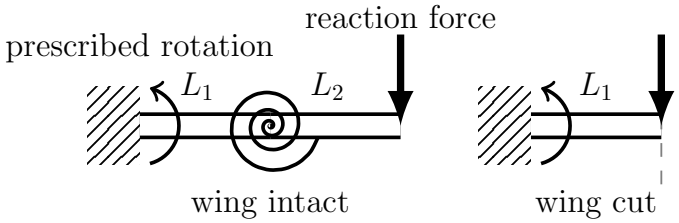

FIGURE 4. SCHEMATIC OF STATIC TESTS USED TO IDENTIFY WING'S YOUNG'S MODULUS AND COSTAL BREAK TORSIONAL STIFFNESS.

structure and base our estimates of A and I from its geometry. Using ImageJ to analyze our images, we found that the leading edge vein's effective diameter ranged from roughly 200 μm near the wing base to 70 μm near the wing tip. We assume that the vein cross section is circular and has a diameter of 100 μm. In practice, the vein cross sectional geometry is complex and variable.

To determine the wing's Young's modulus and costal break torsional stiffness, we conduct a series of force-deflection tests (Fig. 4) on a wing separate from that used during slide preparation. The base of the wing was clamped using a 3D printed fixture (Fig. 5), and the clamping fixture was subsequently attached to a manual rotation stage (0.1° resolution) such that we could impose an angular displacement to the wing base. To measure the reaction forces resulting from base rotation, we placed a load cell (Transducer Techniques, GSO-10, 0.05 mN resolution) near the tip of the wing. We rotated the wing in one-degree increments until it buckled, and subsequently rotated the wing back to its initial orientation. We recorded the force versus angular displacement curve during both the loading and unloading phase. We conducted this process for the (1) intact wing, with the load

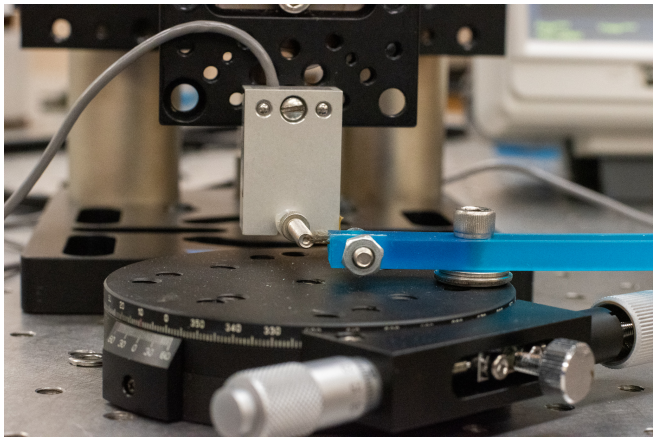

FIGURE 5. EXPERIMENTAL SETUP OF WING IN 3D PRINTED CLAMP FIXED TO ROTATION STAGE.

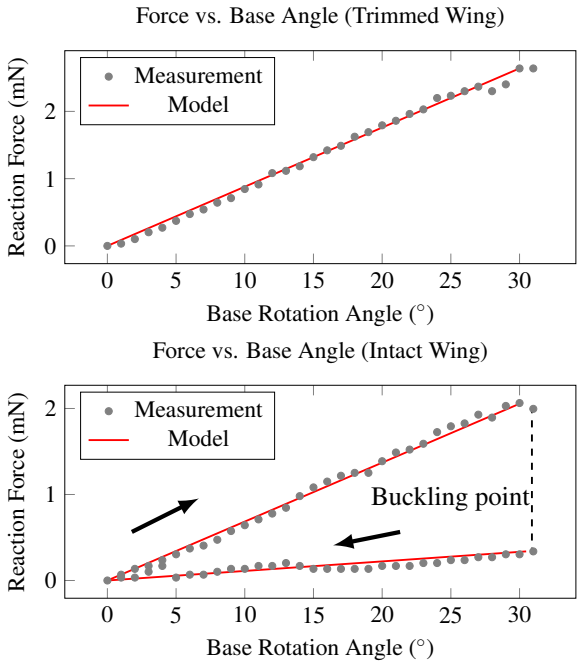

FIGURE 6. FORCE-DISPLACEMENT TESTS FOR INTACT AND TRIMMED YELLOWJACKET WING.

cell placed distal to the costal break, and (2) a wing that had been trimmed at the costal break, with the load cell placed near the end of the remaining wing segment (Fig. 4). Assuming both beams have uniform material properties, cross-sectional area and area moment of inertia, we are able to estimate E by quantifying the force-deflection curve of the trimmed wing (Fig. 6, top). Once E is known, we estimate K_T and αK_T through the force-deflection curve of the intact wing (Fig. 6, bottom).

Model parameters estimated through static testing are shown in Table 1. The Young's modulus falls within the lower end of range for dried insect cuticle (the primary material constituent of vein), though this modulus range varies substantially [21]. We note that our estimate of E is sensitive to the approximated vein diameter t, since the area moment of inertia and consequently the beam's flexural stiffness scale with t^4. We found that the costal break's pre-buckling stiffness in the dried wing was about twice as high as that measured in a fresh wing [14], and were unable to find a comparison for post-buckling stiffness in either fresh or dried wing. Since we did not measure the joint angle directly, but rather the angle between the rotation stage and the wing tip, we used our model to estimate the critical buckling angle. We found that the dried wing buckled at an angle approximately double that of a fresh wing [14]. The beam density was estimated from values published in the literature [22].

TABLE 1. ESTIMATED MODEL PARAMETERS.

Property	Symbol	Value	Unit
Young's Modulus	E	1.403	GPa
Cost. Break Stiffness	k_T	7.0	$\frac{\text{mN-mm}}{\text{rad}}$
Post-buckle scaling factor	α	0.11	-
Length one	L_1	2.85	mm
Length two	L_2	2.81	mm
Diameter	t	100	μm
Cross-sectional area	A	0.0079	mm^2
Area moment of inertia	I	4.91×10^{-6}	mm^4
Density	ρ	1000	kg/m^3
Critical buckling angle	θ_c	19.1	degrees

DYNAMIC SIMULATIONS

We use numerical simulation to better understand the wing's dynamics. We begin by finding the wing's natural frequencies and mode shapes. Then, we estimate the stress distribution in the wing subject to a collision and identify how the presence of the costal break influences this distribution. We also evaluate the reaction torques at the base of the wing as a proxy for stability.

First, we calculate the wing's normal modes (Fig. 7) and natural frequencies by determining the eigenvectors and eigenvalues of $\mathbf{M}^{-1}\mathbf{K}$. The first natural frequency of a homogeneous wing (no costal break) is 517 Hz, while the first natural frequency of the wing with costal break is 798 Hz and 494 Hz in its pre and post-buckled state, respectively. The yellowjacket wingbeat frequency is about 150 Hz [11]. This implies that the costal break, at least before buckling, stiffens the beam assembly and is stiffer than the beam sections immediately surrounding it. As a result, beam's angle of rotation instantaneously decreases at the costal break location when viewed from wing root to tip. By contrast, buckling of the costal break lowers the overall stiffness of the wing, and the buckled costal break has a lower stiffness than the surrounding beam sections. The beam's angle of rotation therefore increases at the costal break location. If the costal break stiffness were to be further reduced, it would eventually behave as a hinge. The first natural frequency would then be zero and correspond to rigid body rotation of the distal portion of the wing.

Wing stresses

Next, we simulate the response of the wing (with and without the costal break) subject to a large impulsive force in order to identify how the costal break affects wing stress. This loading is idealized from what the insect would experience in flight, where the wing would have some non-zero initial velocity profile and

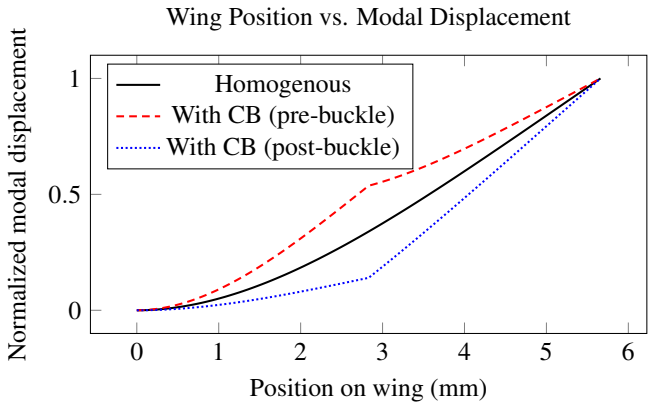

FIGURE 7. MODE SHAPES OF HOMOGENEOUS BEAM AND BEAM WITH COSTAL BREAK (PRE AND POST BUCKLE). CB = COSTAL BREAK.

the point of contact may stick to the object it strikes. We assume the load $F(t)$ is applied at the tip of the wing at length $L_1 + L_2$ and is described by a half-sine wave modulated by the heaviside function $U(t)$, or

$$F(t) = F_{max} \sin\left(\pi \frac{t}{t_d}\right) [U(t) - U(t - t_d)] \tag{13}$$

where F_{max} is the force magnitude and t_d is the duration over which the force is applied. To select F_{max} and t_d, we use the impulse-momentum principle. We consider the wing to be rigid immediately before impact with an angular velocity ω = 942 rad/sec (150 Hz). Following impact, the wing has a zero angular velocity. The impulse-relationship gives

$$\int_0^{t_d} F(t)dt = \frac{I_0 \omega}{L_1 + L_2} \tag{14}$$

where I_0 is the wing's moment of inertia about its left edge. Thus, F_{max} and t_d must be inversely proportional to one another if the impulse is to be fixed. We select an impact duration of t_d = 66.7 μs, which is about 1% the duration of the total wingbeat, and a force magnitude of F_{max} = 1.86 mN.

We use MATLAB's 'lsim' command to simulate the wing response at a time interval of 5 μs over a total time of 2.5 ms which results in 500 time steps. We determined the response of the wing with and without the costal break. For the current load magnitude and duration, we found that the wing with costal break did not buckle if the critical buckling angle was 19.1 degrees. Thus, we also simulated the response of a wing with costal break where the critical buckling angle was reduced to 12.5 degrees, which caused the wing to buckle. Once the wing's dynamic response was calculated, we evaluated stress.

The spatiotemporal stress profiles for the three cases are shown in Fig. 8. We refer to the cases as homogeneous, no-buckle and buckled wings for simplicity. Data is shown only until 1 ms, where the costal break reset to its zero angle for the buckled wing. Peak stresses gradually reduced over the subsequent 1.5 ms interval as the system's oscillations decayed due to damping. The homogeneous wing and no-buckle wing experienced the largest stress near the wingtip where the load was applied. Maximum stresses occurred at the costal break for the

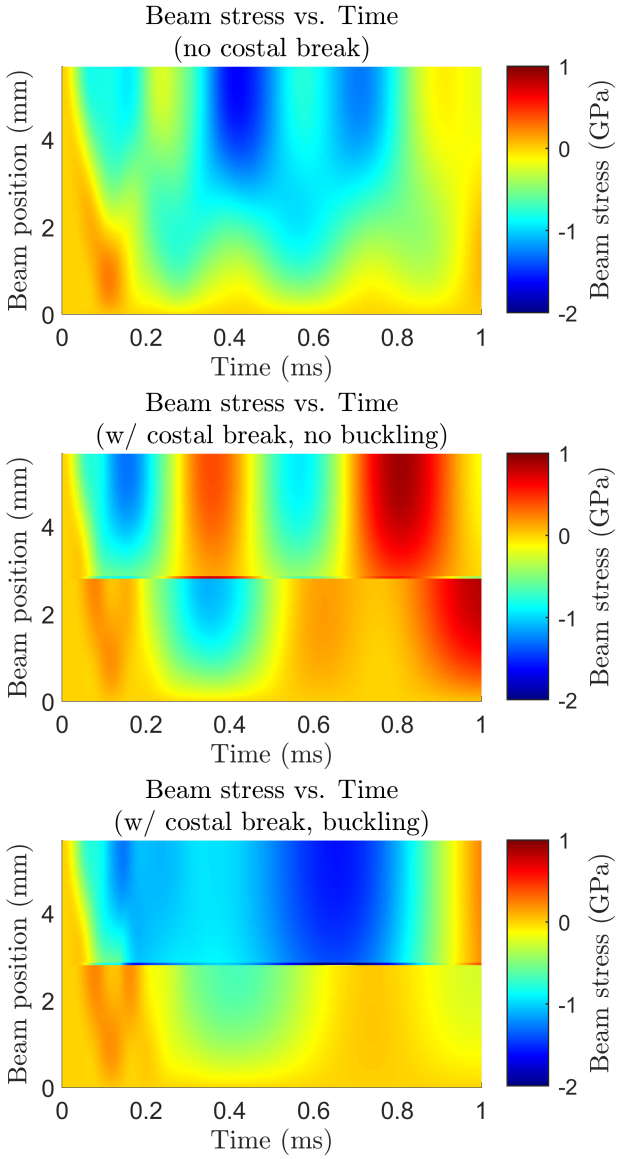

FIGURE 8. SPATIOTEMPORAL STRESS PROFILES FOR A (TOP) HOMOGENEOUS WING, (MIDDLE) WING WITH COSTAL BREAK AND NO BUCKLING, AND (BOTTOM) WING WITH COSTAL BREAK AND BUCKLING.

buckled wing, likely because the costal break in its post-buckled state is less stiff relative to the surrounding beam. By comparison, the unbuckled costal break experiences lower stresses since it is stiffer than the surrounding beam. The no-buckle wing sees the lowest peak stress in general, because it is stiffer than the other two configurations as evidenced by its increased natural frequency. This suggests that the costal break may reduce the peak stresses the wing experiences during normal flapping. Aside from the increased stress at the costal break, the homogeneous and no-buckle wing experience similar peak stresses. The no-buckle wing experiences lower stresses near the wing root, but incurs high peak stresses for a longer duration near the wing tip.

Together, these results suggest that the costal break may reduce wing stress during flight but not necessarily during impact. However, under more realistic collision, we believe the costal break likely does reduce peak stresses. When a wing collides with a fixed obstacle, the collision is generally inelastic. The insect continues to drive its wing through the obstacle until the wing ultimately clears the obstacle. In this case, where the base of the wing is prescribed large rigid body rotation, buckling at the costal break would allow the wing to clear the obstacle earlier in the stroke phase. The duration during which the wing experiences external forcing would simply be shorter.

Reaction Moments

Lastly, we investigate how the costal break affects an insect's flight stability during collision. During collision, an object imparts a large force on the wing. That force causes a reaction moment at the base of the wing which may cause the insect's body to spin, thereby compromising its flight stability. We maintain the same parameters used in the previous numerical simulation. We determine the response for the homogeneous, no-buckle and buckled wing and compute reaction moments at the base of the wing, where the wing meets the insect's body.

Reaction moments for the three cases are shown in Fig. 9. Both the first and second modes contribute to the reaction moments of the homogeneous wing, whereas the first mode dominates the reaction moments of the wing's equipped with the costal break. The homogeneous wing experiences the largest reaction moment of about 2.5 mN-mm. The unbuckled costal break reduces the reaction moment by about 14%, while costal break buckling reduces the reaction moment by 32%. We can also calculate the angular impulse of the reaction moment, where the angular impulse provides a better estimate of how much the costal break would reduce the insect body angular velocity following a collision. We consider an interval $0 < t < 0.15$ ms, where the upper bound was selected because the reaction moments of the homogeneous and buckled wing approach zero. Over this interval, the angular impulse caused by the reaction moment is 0.082 N-mm-ms and 0.046 N-mm-ms for the homogeneous and buckled

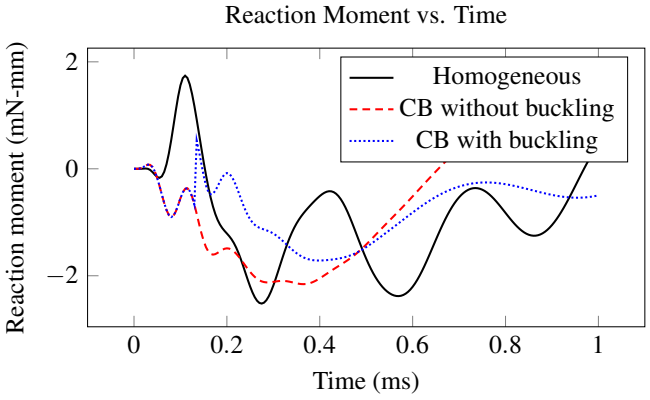

FIGURE 9. REACTION MOMENTS FOR A HOMOGENEOUS WING, WING WITH COSTAL BREAK AND NO BUCKLING, AND WING WITH COSTAL BREAK AND BUCKLING. CB = COSTAL BREAK.

wings respectively. This suggests that the angular rate imposed to the insect body at the end of this interval is reduced by about 46% due to the presence of the costal break.

DISCUSSION

While this simple model provides insight into the costal break, there are several factors that must be considered moving forward to better understand its dynamics. First, we must acquire a more accurate representation of the insect wing. Wings are complex structures with spatially varying geometry and material properties. Material properties rely critically on hydration, and thus mechanical testing on wings removed from deceased insects may distort property absolute values. Moving forward, we must better characterize how the material and geometric properties vary in space on fresh wings. Further, we must conduct dynamic testing on the costal break to determine whether or not rate-dependent effects influence its behavior. While the quasi-static tests conducted in this research demonstrate hysteresis, it is plausible that time-dependent force-displacement testing will change the characteristics of this hysteresis. Finally, we require a more accurate representation of the collision itself. Wings often collide with objects inelastically, and the insect continues to drive the base of its wing until the wing loses contact and passes the obstacle. From a modeling perspective, this implies the wing has a non-zero initial velocity field, and is prescribed a large rigid body rotation at the base of the wing. We believe that modeling the collision in this way would more accurately represent the costal break's potential to prevent wing damage and enhance flight stability.

CONCLUSION

In this research, we developed a simple model of an insect wing with costal break. The model consisted of two homogeneous

beams interconnected by a torsional spring, where the torsional spring stiffness changed instantaneously once it had exceeded a critical angle. We carried out static tests on a yellowjacket wing to determine model parameters and used numerical simulation to predict the wing's response after a collision. We found that the costal break reduced stresses in the wing if the costal break did not buckle. If the costal break did buckle, stresses in the wing were comparable to a homogeneous wing without a costal break. In practice, buckling would likely allow the wing to clear an obstacle more quickly during an inelastic collision, which may reduce the damage a wing experiences. We found that wing buckling reduced the reaction moments at the insect body as much as 32% compared to the reaction moments experienced by a homogeneous wing. This result suggests that the costal break may improve the insect's flight stability by reducing the insect body's rate of rotation following a collision, which agrees with studies conducted on free flying robotic insects [14].

ACKNOWLEDGMENT

This research was supported the National Science Foundation under awards Nos. CBET-1855383 and CMMI-1942810 to MJ. Any opinions, findings, and conclusions or recommendations expressed in this material are those of the author(s) and do not necessarily reflect the views of the National Science Foundation.

REFERENCES

[1] Dickinson, M. H., Lehmann, F.-O., and Sane, S. P., 1999. "Wing rotation and the aerodynamic basis of insect flight". *Science,* ***284***(5422), pp. 1954–1960.

[2] Tian, F.-B., Luo, H., Song, J., and Lu, X.-Y., 2013. "Force production and asymmetric deformation of a flexible flapping wing in forward flight". *Journal of Fluids and Structures,* ***36***, pp. 149–161.

[3] Reid, H. E., Schwab, R. K., Maxcer, M., Peterson, R. K., Johnson, E. L., and Jankauski, M., 2019. "Wing flexibility reduces the energetic requirements of insect flight". *Bioinspiration & biomimetics,* ***14***(5), p. 056007.

[4] Dickerson, B. H., Aldworth, Z. N., and Daniel, T. L., 2014. "Control of moth flight posture is mediated by wing mechanosensory feedback". *Journal of Experimental Biology,* ***217***(13), pp. 2301–2308.

[5] Dukas, R., and Dukas, L., 2011. "Coping with nonrepairable body damage: effects of wing damage on foraging performance in bees". *Animal behaviour,* ***81***(3), pp. 635–638.

[6] Cartar, R. V., 1992. "Morphological senescence and longevity: an experiment relating wing wear and life span in foraging wild bumble bees". *Journal of Animal Ecology*, pp. 225–231.

[7] Combes, S., Crall, J., and Mukherjee, S., 2010. "Dynamics of animal movement in an ecological context: dragonfly wing damage reduces flight performance and predation success". *Biology letters,* ***6***(3), pp. 426–429.

[8] Haas, C., and Cartar, R., 2008. "Robust flight performance of bumble bees with artificially induced wing wear". *Canadian journal of zoology,* ***86***(7), pp. 668–675.

[9] Lyu, Y. Z., Zhu, H. J., and Sun, M., 2020. "Wing kinematic and aerodynamic compensations for unilateral wing damage in a small phorid fly". *Physical Review E,* ***101***(1), p. 012412.

[10] Foster, D. J., and Cartar, R. V., 2011. "What causes wing wear in foraging bumble bees?". *Journal of Experimental Biology,* ***214***(11), pp. 1896–1901.

[11] Mountcastle, A. M., and Combes, S. A., 2014. "Biomechanical strategies for mitigating collision damage in insect wings: structural design versus embedded elastic materials". *Journal of Experimental Biology,* ***217***(7), pp. 1108–1115.

[12] Rajabi, H., Dirks, J.-H., and Gorb, S. N., 2020. "Insect wing damage: causes, consequences and compensatory mechanisms". *Journal of Experimental Biology,* ***223***(9).

[13] Danforth, B. N., and Michener, C. D., 1988. "Wing folding in the hymenoptera". *Annals of the Entomological Society of America,* ***81***(2), pp. 342–349.

[14] Mountcastle, A. M., Helbling, E. F., and Wood, R. J., 2019. "An insect-inspired collapsible wing hinge dampens collision-induced body rotation rates in a microrobot". *Journal of the Royal Society Interface,* ***16***(150), p. 20180618.

[15] Mintchev, S., de Rivaz, S., and Floreano, D., 2017. "Insect-inspired mechanical resilience for multicopters". *IEEE Robotics and automation letters,* ***2***(3), pp. 1248–1255.

[16] Rizos, P., Aspragathos, N., and Dimarogonas, A., 1990. "Identification of crack location and magnitude in a cantilever beam from the vibration modes". *Journal of sound and vibration,* ***138***(3), pp. 381–388.

[17] Liang, R. Y., Choy, F. K., and Hu, J., 1991. "Detection of cracks in beam structures using measurements of natural frequencies". *Journal of the Franklin Institute,* ***328***(4), pp. 505–518.

[18] Kindova-Petrova, D., 2014. "Vibration-based methods for detecting a crack in a simply supported beam". *Journal of Theoretical and Applied Mechanics,* ***44***(4), pp. 69–82.

[19] Rao, S. S., 2007. *Vibration of continuous systems*, Vol. 464. Wiley Online Library.

[20] Logan, D. L., 2017. *A first course in the finite element method*. Nelson Education.

[21] Klocke, D., and Schmitz, H., 2011. "Water as a major modulator of the mechanical properties of insect cuticle". *Acta biomaterialia,* ***7***(7), pp. 2935–2942.

[22] Vincent, J. F., and Wegst, U. G., 2004. "Design and mechanical properties of insect cuticle". *Arthropod structure & development,* ***33***(3), pp. 187–199.